Taylor & Francis
Taylor & Francis Group

The hydrogen storage capacity of coinage metalated benzenes studied by DFT

Athanassios C. Tsipis & Dimitrios N. Gkarmpounis

View supplementary material 🗗

Accepted author version posted online: 22 Jun 2015.
Published online: 13 Jul 2015.

Submit your article to this journal 🗗

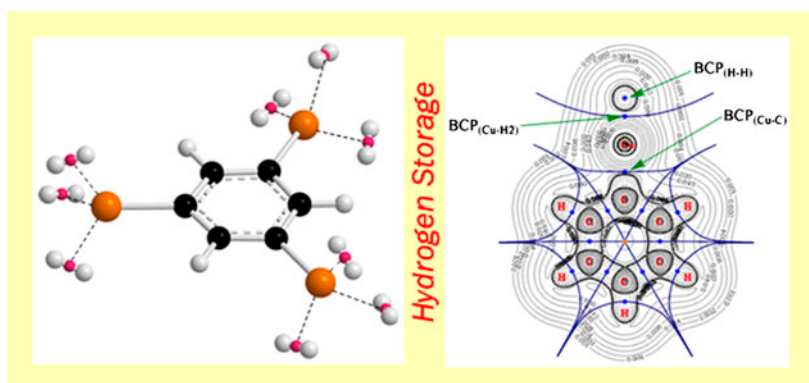Article views: 59

View related articles 🗗

View Crossmark data 🗗

Taylor & Francis
Taylor & Francis Group

The hydrogen storage capacity of coinage metalated benzenes studied by DFT

ATHANASSIOS C. TSIPIS* and DIMITRIOS N. GKARMPOUNIS

Laboratory of Inorganic and General Chemistry, Department of Chemistry, University of Ioannina, Ioannina, Greece

The hydrogen storage capacity of representative cuprated benzenes (C_6H_5Cu and $1,3,5$-$Cu_3C_6H_3$ molecules) has been investigated by DFT calculations and found to fulfill the US department of energy target requirements for low-cost hydrogen storage materials. A thorough analysis of the bonding $Cu\cdots(\eta^2$-$H_2)$ interactions by a multitude of electronic structure calculation methods (natural bond orbital, AIM, electron localization function, reduced density gradient, and $Sign(\lambda_2(\mathbf{r}))\rho(\mathbf{r})$ functions) showed that these interactions exhibit a mixed covalent-ionic character accompanied by weak intermolecular dispersion interactions as well.

Keywords: Phenylcopper; $1,3,5$-$Cu_3C_6H_3$ molecule; Hydrogen storage capacity; DFT; Bonding $Cu\cdots(\eta^2$-$H_2)$ interactions

1. Introduction

The design of new materials for hydrogen storage continues to be a major research area for the development of future hydrogen energy applications driven to a large extent by technological demands, especially for mobile applications [1]. The prime goal for "The Hydrogen Economy" [2] to be realized is that of inventing safe, efficient, and effective storage for H_2

---

*Corresponding author. Email: attsipis@uoi.gr

gas, and to replace current technologies based around the compression of H_2 as a liquid or as a gas using cryogenic temperatures or high pressures [2(a)]. Therefore, there is major worldwide interest in meeting the United States Department of Energy (DOE) targets of 6.5% w/w gravimetric and 45 g L^{-1} volumetric H_2 storage by 2010, and 9.0% w/w and 81 g L^{-1} by 2015 for mobile applications [3].

Hydrogen storage materials could be divided into two classes depending on the mechanism of hydrogen sorption: materials where adsorption is due to physisorption or due to chemisorption. In the case of physisorption, molecular hydrogen is weakly bound to the surface of the material by van der Waals or hydrogen bonds. In the case of chemisorption, H_2 molecules dissociate into atomic hydrogen which is then absorbed into the bulk, forming stronger ionic or covalent bonds with the material. An ideal storage system would be one where hydrogen binds molecularly but with a binding energy that is intermediate between the physisorbed and the chemisorbed state.

Transition metal (TM) atoms interacting with H_2 molecules form dihydrogen complexes through the so-called Kubas interaction [4]. This bonding mode offers a rare opportunity for the development of reversible hydrogen storage media for near room temperature operation [5], because the binding energy of the H_2 molecule in the system is theoretically estimated to be in the range of 0.2–0.6 eV [6]. A good contender for hydrogen storage through the Kubas interactions should be of comparatively low molecular weight, cheap and should be further capable of rapid adsorption–desorption kinetic behavior which simulates an effective capturing and removal process [1(f)]. An alternative for chemical hydrogen storage is provided by materials storing hydrogen as hydridic/protonic H combined with other elements (e.g., B, C, and N). An exhaustive list of this class of chemical hydrogen storage materials is given by Demirci and Miele [1(g)]. Hydrogen storage in metal hydrides has also been the focus of intensive research. For example, magnesium dihydride combines a high H_2 capacity of 7.7% w/w with the benefit of the low cost of the abundantly available magnesium [7]. In metal hydrides, the hydrogen–metal interactions correspond to a direct σ metal hydride bond, in which the hydrogen shares its 1s electron with one of the available valence electrons of the metal and can give four basic hydride species: MH, MH_2, MH_3, and MH_4 [8]. Depending on the properties of the metal atom involved mixed hydride/dihydrogen complexes formulated as $MH_x(H_2)_y$ ($x = 1–4$; $y = 0–6$) may be also formed. A combined experimental and theoretical study of the $MH_x(H_2)_y$ species (M = La–Gd; $x = 1–4$; $y = 0–6$) has recently been reported by Gagliardi and coworkers [8].

Metalated benzenes and particularly lithiated benzenes, aside from being very powerful reagents in organic synthesis, are of particular interest in fundamental research and quite a lot of theoretical work has been devoted to determination of their structures, relative stabilities of their isomers, as well as of various other intriguing properties. Very recently, Giri *et al.* [9] investigated by DFT and *ab initio* molecular dynamics calculations the possibility of using star-like hexalithiobenzene as a hydrogen storage material. Calculations predicted that hexalithiobenzene could be a good candidate to serve as hydrogen storage material which can efficiently absorb hydrogen in its molecular form at low temperature and desorb it at room temperature. C_6Li_6 can trap 6–12 H_2 molecules in molecular form with a good gravimetric weight percentage (9.6% w/w for $H_2@C_6Li_6$) [1(f)].

Group 11 coinage metals (Cu, Ag, and Au) are also known to metalate benzene. Phenylcopper, C_6H_5Cu, is the first organocopper compound and its synthesis was reported by Reich in 1923 as an impure product obtained in 60% yield from phenylmagnesium bromide and cuprous iodide in ether [10]. Since then, several other methods for synthesis of C_6H_5Cu have been reported [11]. Phenylcopper as well as its clusters are widely used as

reagents in organic synthesis [12]. Since 1923, several unsuccessful attempts were made to synthesize and isolate phenylsilver, C_6H_5Ag [13], until Beverwijk *et al.* [14] synthesized, isolated, and characterized phenylsilver as one of the most stable unfluorinated σ-bonded organosilver compounds known at that time. Finally, phenylgold, C_6H_5Au, has also been synthesized and along with its silver counterpart, C_6H_5Ag, as well as their anions $[AuC_6H_5]^-$ and $[AgC_6H_5]^-$ have been studied by Sun *et al.* [15] employing photoelectron spectroscopy and DFT calculations. In subsequent work, Liu *et al.* [16] employed the same techniques and methods to study the structure and formation mechanism of $[C_6H_5Cu_m]^-$ ($m = 1$–3). The structure and the formation mechanism of the silver and gold counterparts, $[C_6H_5M_m]^-$ (M = Ag or Au, $m = 1$–3), have also been studied in detail using DFT calculations at the B3LYP//6-311G(d,p)/Lanl2dz level of theory [17].

Continuing our interest on the study of coinage metalated benzenes [18], we set out to explore herein by electronic structure calculation methods the hydrogen storage capacity of coinage metalated benzenes and the potential for using these molecules as hydrogen storage materials.

2. Computational details

All calculations were performed using the Gaussian09 program suite [19]. The geometries of all stationary points were fully optimized, without symmetry constraints, employing the 1999 hybrid functional of Perdew *et al.* [20] denoted as PBE0 as implemented in the Gaussian09 program suite [19]. For the geometry optimizations, we used the Def2-QZVPP basis set for all atoms. Hereafter, the method used in DFT calculations is abbreviated as PBE0/Def2-QZVPP. The selection of the PBE0 density functional was based on the fact that PBE0 (PBE1PBE) generally gives the best results for various properties of TM and main group element compounds [21]. Def2-QZVPP basis set is a high-quality basis set providing smaller mean errors for a variety of computed properties of TM and main group compounds [22]. All stationary points have been identified as minima. The natural bond orbital (NBO) population analysis was performed using Weinhold's methodology as implemented in the NBO 6.0 software [23]. Magnetic shielding tensors have been computed with the GIAO (gage-including atomic orbitals) DFT method [24, 25] as implemented in the Gaussian09 series of programs [19] employing the PBE0 functional (abbreviated as GIAO-BPE0/Def2-QZVPP method). Topological and energetic properties of $\rho(\mathbf{r})$ at the (3,−1) bond critical points (BCPs) were calculated by means of the Bader's [26] Quantum theory of atoms in molecules (QTAIM) methodology. The 2-D plots of the electron localization function (ELF) and the real space $Sign(\lambda_2(\mathbf{r}))\rho(\mathbf{r})$ function with promolecular approximation as well as the 3-D surfaces of the reduced density gradient (RDG) were obtained employing the Multiwfn software version 3.2. [27]. The λ_2 term in the $Sign(\lambda_2(\mathbf{r}))\rho(\mathbf{r})$ function is obtained as the second largest eigenvalue of the averaged electron density Hessian matrix computed through the dynamical trajectory. The adaptive natural density partitioning (AdNDP) [28] calculations were employed as implemented in the Multiwfn 3.2.

3. Results and discussion

3.1. *Hydrogen storage capacity of phenylcopper, C_6H_5Cu*

First, we explored the hydrogen storage capability of phenylcopper, C_6H_5Cu, investigating the copper–H_2 interactions by electronic structure calculation methods. Figure 1 shows the
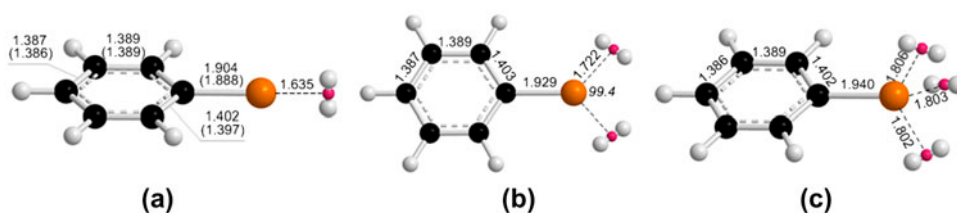
Figure 1. Optimized geometries and selected structural parameters of the (a) $C_6H_5Cu(\eta^2-H_2)$, (b) $C_6H_5Cu(\eta^2-H_2)_2$, and (c) $C_6H_5Cu(\eta^2-H_2)_3$ species calculated at the PBE0/Def2-QZVPP level of theory (numbers in parenthesis refer to structural parameters calculated for the parent C_6H_5Cu molecule).

PBE0/Def2-QZVPP optimized geometries along with selected structural parameters of the $C_6H_5Cu(H_2)_n$ ($n = 1$–3) molecules. Notice that all our attempts to load the copper center with four H_2 molecules were unsuccessful, since in the resulting optimized geometries, the fourth H_2 molecule was always far apart from copper.

In $C_6H_5Cu(H_2)$, H_2 is coordinated to Cu through a side-on coordination mode (η^2 coordination mode) adopting a perfect vertical orientation relative to the carbocyclic ring plane. The distance between the copper and the centroid of the H–H bond, Cu–cd(H–H), is 1.635 Å. Generally, the structural integrity and planarity of the carbocyclic ring are retained in $C_6H_5Cu(\eta^2-H_2)$. The most significant structural change undergoing the C_6H_5Cu moiety upon interaction with H_2 is elongation of the C–Cu bond by 0.016 Å. It can also be seen that the H–H bond of the coordinated H_2 molecule in the $C_6H_5Cu\cdots(\eta^2-H_2)$ complex is elongated by 0.044 Å.

The BSSE-corrected interaction energy (IE), for the $C_6H_5Cu\cdots(\eta^2-H_2)$ interaction is calculated to be equal to 13.8 kcal mol^{-1} at the PBE0/Def2-QZVPP level. According to the US DOE targets for hydrogen storage applications, the binding energy (or IE) per H_2 molecule, which is sometimes also referred to as the removal energy or equivalently the absorption energy, should be in the range of 0.7–0.2 eV (or 16.1–4.6 kcal mol^{-1}) [29]. Obviously, the estimated IE for $C_6H_5Cu\cdots(\eta^2-H_2)$ is within the US DOE targets. Upon attaching a second H_2 molecule to $C_6H_5Cu(\eta^2-H_2)$, a further elongation of the C–Cu bond by 0.046 Å is observed and the total elongation with respect to C–Cu bond length found in C_6H_5Cu is 0.062 Å. The elongation of the two H–H bonds in $C_6H_5Cu(\eta^2-H_2)_2$ is 0.045 Å and it is almost the same as that found for $C_6H_5Cu(\eta^2-H_2)$. The coordinated H_2 molecules in $C_6H_5Cu(\eta^2-H_2)_2$ are further away from the metal center with Cu-cd(H–H) distances calculated equal to 1.722 Å. Nonetheless, the structural parameters of the carbocyclic ring remain practically unaffected. The $C_6H_5Cu(\eta^2-H_2)_2$ complex adopts a trigonal planar arrangement of the two H_2 ligands and the phenyl ligand. The BSSE-corrected IE for the attachment of the second H_2 molecule to copper is calculated to be 7.9 kcal mol^{-1}, which is again within the US DOE targets. Attachment of a third H_2 molecule to the copper results in a pseudo-tetrahedral arrangement of the ligands around the metal center. In the $C_6H_5Cu(\eta^2-H_2)_3$ complex, the C–Cu bond and the Cu–cd(H–H) distances are the longest compared to those found for the complexes bearing one and two H_2 molecules. Thus, the C–Cu bond in $C_6H_5Cu(\eta^2-H_2)_3$ is calculated to be 1.940 Å, elongated by 0.073 Å with respect to that found in C_6H_5Cu, while the Cu–cd(H–H) distances are calculated to be more than 1.8 Å. However, it should be noticed that the structural parameters of the carbocyclic ring are almost unaltered upon attachment of three H_2 molecules to the copper metal center. Finally, the IE of the third H_2 molecule with $C_6H_5Cu(\eta^2-H_2)_2$ is calculated to be 5.6 kcal mol^{-1},

once more within the US DOE targets. Overall, the average IE per H_2 molecule in C_6H_5Cu $(\eta^2-H_2)_3$ is 9.1 kcal mol^{-1}. Noteworthy is the remarkable stabilization of C_6H_5Cu under a hydrogen atmosphere.

The theoretical gravimetric capacities for $C_6H_5Cu(\eta^2-H_2)$, $C_6H_5Cu(\eta^2-H_2)_2$, and C_6H_5Cu $(\eta^2-H_2)_3$ are 1.4, 2.8, and 4.1% w/w, respectively, falling below the US DOE gravimetric capacity target for 2015 which is 5.5% w/w [28]. On the other hand, the volumetric capacities of $C_6H_5Cu(\eta^2-H_2)$, $C_6H_5Cu(\eta^2-H_2)_2$, and $C_6H_5Cu(\eta^2-H_2)_3$, based on molecular volume calculations, are 24, 41, and 50 g L^{-1}, respectively. Again, these numbers are below the US DOE volumetric capacity target for 2015 which is 70 g L^{-1}. [30] Accordingly, we explored the H_2 storage capacity of the other coinage metalated benzenes bearing more than one metal atom. Due to the US DOE target for low-cost materials, we have only focused on the systems bearing copper for obvious reasons. Among all the coinage metalated species bearing more than one copper, it is found that the best potential candidate to be examined as a H_2 storage material is the $1,3,5-Cu_3C_6H_3$ molecule.

3.2. *Hydrogen storage capacity of $1,3,5-Cu_3C_6H_3$ molecule*

The optimized structures along with selected structural parameters of $1,3,5-Cu_3C_6H_3$ gradually loaded with three, six, and up to nine H_2 molecules calculated at the PBE0/Def2-QZVPP level are shown in figure 2. Attempts to load $1,3,5-Cu_3C_6H_3$ with more than nine H_2 molecules were unsuccessful, since the extra H_2 molecules were always away from the copper centers.

Perusal of figure 2 reveals that the H_2 molecules are attached to copper of the $1,3,5-Cu_3C_6H_3$ species in a similar way as that found in the C_6H_5Cu species, i.e., with a η^2 fashion adopting vertical, trigonal planar, and tetrahedral arrangement around the metal centers in the $1,3,5-C_6H_3Cu(\eta^2-H_2)Cu(\eta^2-H_2)Cu(\eta^2-H_2)$, $1,3,5-C_6H_3Cu(\eta^2-H_2)_2Cu(\eta^2-H_2)_2$ $Cu(\eta^2-H_2)_2$, and $1,3,5-C_6H_3Cu(\eta^2-H_2)_3Cu(\eta^2-H_2)_3Cu(\eta^2-H_2)_3$ complexes, respectively. The calculated Cu–cd(H–H) distances are slightly elongated compared to those found in the respective $C_6H_5Cu(\eta^2-H_2)$, $C_6H_5Cu(\eta^2-H_2)_2$, and $C_6H_5Cu(\eta^2-H_2)_3$ complexes. In contrast,
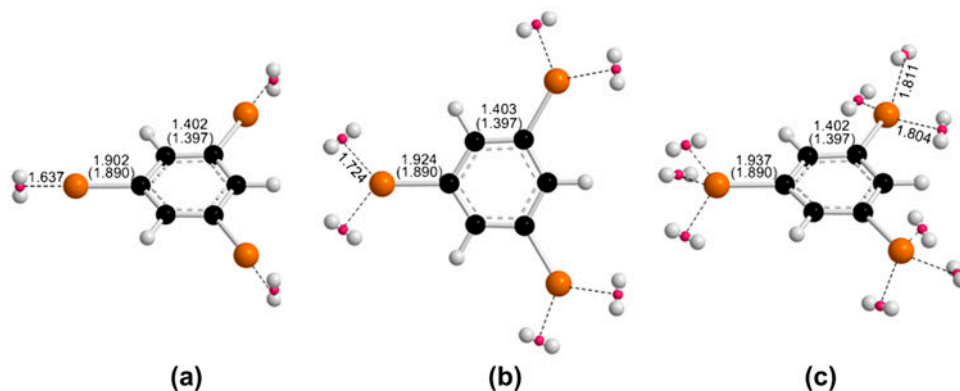
Figure 2. Optimized geometries and selected structural parameters of the (a) $1,3,5-C_6H_3Cu(\eta^2-H_2)Cu(\eta^2-H_2)Cu$ (η_2-H_2), (b) $1,3,5-C_6H_3Cu(\eta^2-H_2)_2Cu(\eta^2-H_2)_2Cu(\eta_2-H_2)_2$, and (c) $1,3,5-C_6H_3Cu(\eta^2-H_2)_3Cu(\eta^2-H_2)_3Cu(\eta_2-H_2)_3$ complexes calculated at the PBE0/Def2-QZVPP level (numbers in parenthesis refer to structural parameters of $1,3,5-C_6H_3Cu_3$).

upon attachment of H_2 molecules, the C–Cu bonds in $1,3,5\text{-}C_6H_3Cu(\eta^2\text{-}H_2)Cu(\eta^2\text{-}H_2)Cu(\eta^2\text{-}H_2)$, $1,3,5\text{-}C_6H_3Cu(\eta^2\text{-}H_2)_2Cu(\eta^2\text{-}H_2)_2Cu(\eta^2\text{-}H_2)_2$, and $1,3,5\text{-}C_6H_3Cu(\eta^2\text{-}H_2)_3Cu(\eta^2\text{-}H_2)_3Cu(\eta^2\text{-}H_2)_3$ are slightly less elongated compared to the C–Cu bond elongation observed for the analogous $C_6H_5Cu(\eta^2\text{-}H_2)_n$ ($n = 1$–3) complexes. Finally, the structural integrity and planarity of the carbocyclic ring is retained with marginal changes of its structural parameters. The interaction energies per H_2 molecule (BSSE included) are 12.7, 6.6, and 4.8 kcal - mol^{-1} for the $1,3,5\text{-}Cu_3C_6H_3$ bearing three, six, and nine H_2 molecules, respectively, and are within the range set by US DOE target. The gravimetric capacities of $1,3,5\text{-}C_6H_3Cu(\eta^2\text{-}H_2)Cu(\eta^2\text{-}H_2)Cu(\eta^2\text{-}H_2)$, $1,3,5\text{-}C_6H_3Cu(\eta^2\text{-}H_2)_2Cu(\eta^2\text{-}H_2)_2Cu(\eta^2\text{-}H_2)_2$, and $1,3,5\text{-}C_6H_3Cu(\eta^2\text{-}H_2)_3Cu(\eta^2\text{-}H_2)_3Cu(\eta^2\text{-}H_2)_3$ are 2.2, 4.3, and 6.3% w/w, respectively, while the respective volumetric capacities are 67, 110, and 98 g L^{-1}. Obviously, the values for the binding energy, the gravimetric as well as the volumetric capacities calculated for the $1,3,5\text{-}Cu_3C_6H_3(\eta^2\text{-}H_2)_9$ species are all above the targets set by the US DOE.

Taking into account the use of the coinage metalated benzenes as potential candidates of materials for H_2 storage, we thought it would be advisable to study in more depth their interaction with H_2 molecules. For the sake of simplicity, we would examine only the species bearing one copper metal center, and for comparison, we would examine also the most promising $1,3,5\text{-}C_6H_3Cu(\eta^2\text{-}H_2)Cu(\eta^2\text{-}H_2)Cu(\eta^2\text{-}H_2)$, $1,3,5\text{-}C_6H_3Cu(\eta^2\text{-}H_2)_2Cu(\eta^2\text{-}H_2)_2Cu(\eta^2\text{-}H_2)_2$, and $1,3,5\text{-}C_6H_3Cu(\eta^2\text{-}H_2)_3Cu(\eta^2\text{-}H_2)_3Cu(\eta^2\text{-}H_2)_3$ complexes. The estimated Wiberg bond orders (WBOs) for the $C_6H_5Cu\cdots(\eta^2\text{-}H_2)$ interaction in the $C_6H_5Cu(\eta^2\text{-}H_2)$,
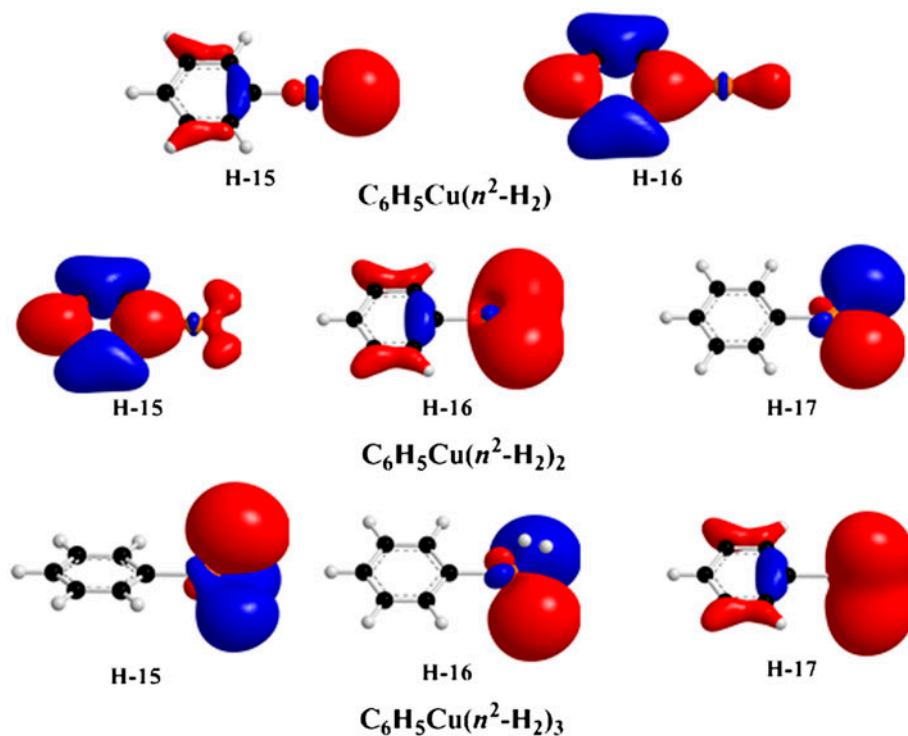
Figure 3. 3-D plots of the MOs relevant to the $C_6H_5Cu\cdots(\eta^2\text{-}H_2)$ interactions in $C_6H_5Cu(\eta^2\text{-}H_2)_n$ ($n = 1$–3) complexes (isocontour value = 0.030).

$C_6H_5Cu(\eta^2\text{-}H_2)_2$, and $C_6H_5Cu(\eta^2\text{-}H_2)_3$ complexes of 0.284, 0.321, and 0.318, respectively, demonstrate weak covalent $Cu\cdots(\eta^2\text{-}H_2)$ interactions. Upon addition of a second H_2 molecule to $C_6H_5Cu(\eta^2\text{-}H_2)$, the WBO increases, while, when adding a third H_2 molecule to the $C_6H_5Cu(\eta^2\text{-}H_2)_2$, the WBO slightly decreases.

The 3-D plots of the MOs relevant to $C_6H_5Cu\cdots(\eta^2\text{-}H_2)$ interactions are shown in figure 3. In $C_6H_5Cu(\eta^2\text{-}H_2)$,two bonding MOs arising from the in-phase combination of the $3d_{z^2}$ AO of copper with the σ bonding MO of the H_2 molecule describe the covalent $C_6H_5Cu\cdots(\eta^2\text{-}H_2)$ interactions. On the other hand, the covalent component of the $C_6H_5Cu\cdots(\eta^2\text{-}H_2)$ interaction in both $C_6H_5Cu(\eta^2\text{-}H_2)_2$ and $C_6H_5Cu(\eta^2\text{-}H_2)_3$ is due to three bonding MOs constructed from the in-phase combination of $3d_{z^2}$ and $3d_{x^2-y^2}$ AOs of Cu with the σ MOs of the coordinated H_2 molecules.

Next, we looked for possible hyperconjugation effects on the $Cu\cdots(\eta^2\text{-}H_2)$ interactions in the $C_6H_5Cu(\eta^2\text{-}H_2)_n$ ($n = 1$–3) complexes. The stabilization energy, $\Delta E(2)$, associated with possible charge transfer (CT) interactions between the relevant donor-acceptor orbitals computed from the second-order perturbative estimates of the Fock matrix in the NBO analysis according to the equation $\Delta E(2) = q_i F_{ij}^2 / \varepsilon_i - \varepsilon_j$ allows specific hyperconjugative interactions to be pinpointed. This equation evaluates the magnitude of the donor–acceptor interaction in terms of the spatial overlap of the NBO, using the off-diagonal Fock-matrix elements F_{ij} and the difference in energy between the NBOs, $\varepsilon_i - \varepsilon_j$, weighted by the occupancy of the donor NBO, q_i. The most significant perturbative donor–acceptor interactions introducing favorable hyperconjugative effects related to the $Cu\cdots(\eta^2\text{-}H_2)$ bonding in the $C_6H_5Cu(\eta^2\text{-}H_2)_n$ ($n = 1$–3) complexes are given schematically in figure 4 along with the respective values of the stabilization energy, $\Delta E(2)$.

Three significant hyperconjugative interactions occur in $C_6H_5Cu(\eta^2\text{-}H_2)$ (figure 4). The first donor–acceptor interaction involves a CT from a bonding NBO of σ-type located on the H_2 molecule toward an antibonding LP* NBO (LP stands for lone pair), which is mainly a p AO of copper. This interaction stabilizes the system by about 15 kcal mol^{-1}. The second donor–acceptor interaction involves a CT from a LP NBO of d-type located on copper toward a BD* (BD stands for bonding) antibonding NBO of σ*-type on H_2 molecule stabilizing the system by almost 13 kcal mol^{-1}. Finally, the third hyperconjucative interaction involves a CT from a bonding NBO of σ-type on coordinated H_2 molecule toward an antibonding BD* NBO localized on the carbon–metal bond, which stabilizes the system by more than 32 kcal mol^{-1}. The total stabilization energy due to the three hyperconjugative interactions in the $C_6H_5Cu(\eta^2\text{-}H_2)$ species is 60.3 kcal mol^{-1}. Therefore, the coordination of H_2 to the Cu center of the $C_6H_5Cu(\eta^2\text{-}H_2)$ molecule could be considered as a "Kubas-type" interaction. The latter involves donation of two electrons from the σ bonding MO of the H_2 molecule to a vacant 3d AO of a metal accompanied by a back-donation of electrons from a filled d AO of the metal to the σ* antibonding MO of the H_2 molecule [4, 31]. However, it should be noticed that in $C_6H_5Cu(\eta^2\text{-}H_2)$ there is donation of electrons from the σ bonding MO of H_2 to a vacant 4p AO of Cu, since all of its 3d AOs are filled, while there is also a back-donation from the 3d AOs of copper to the σ* antibonding MO of H_2. In addition, employment of the AdNDP method [28] revealed the existence of a 3c–2e bond for the $C_6H_5Cu\cdots(\eta^2\text{-}H_2)$ interaction (scheme 1).

The 3c–2e bond is formed from the in-phase interaction of a 3d AO of Cu and the σ MO of H_2. Remarkably, in our systems, there is also a donation of electrons from the σ bonding MO of the H_2 molecule toward a σ* antibonding MO located on the C–Cu bond, which among all three hyperconjugative effects observed, mostly stabilizes the system. The σ*(C–Cu) natural bonding orbital involved in this hyperconjugative interaction is
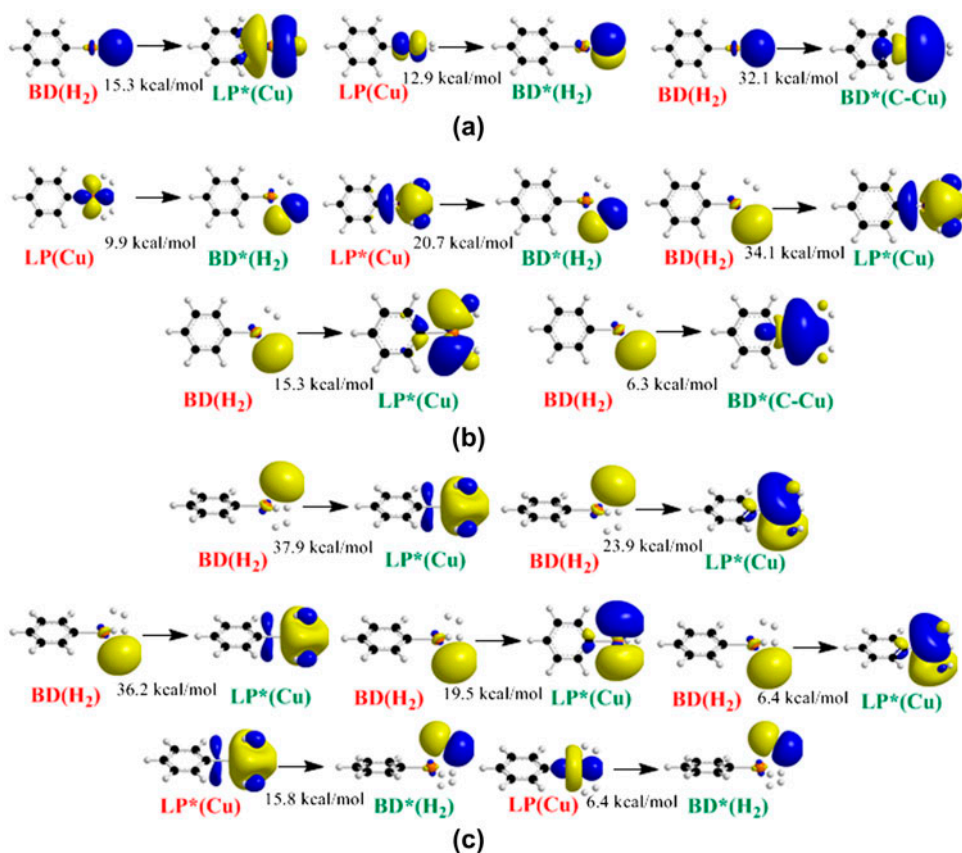
Figure 4. Selected hyperconjugative interactions in (a) $C_6H_5Cu(\eta^2\text{-}H_2)$, (b) $C_6H_5Cu(\eta^2\text{-}H_2)_2$, and (c) $C_6H_5Cu(\eta^2\text{-}H_2)_3$ species (labels of donor and acceptor NBOs are in red and blue, numbers are the respective $\Delta E(2)$ terms) (see http://dx.doi.org/10.1080/00958972.2015.1064906 for color version).

constructed from an sp (74.07% p character) natural hybrid orbital (NHO) on the *ipso* carbon interacting in-phase with an sd (90% s character and 6% d character) NHO of copper, having the form $\sigma^*(C–Cu) = 0.4677\, h_C - 0.8839\, h_{Cu}$. Thus, the elongation of the C–Cu bond of C_6H_5Cu upon interaction with H_2 is probably due to the $\sigma(H–H) \rightarrow \sigma^*(C–Cu)$ electron transfer. Overall, based upon the NBO charges in the $C_6H_5Cu(\eta^2\text{-}H_2)$ species there is a net electron density transfer of 0.07 |e| from H_2 to C_6H_5Cu moiety. The electron density is transferred from the 1σ MO of H_2 toward mainly the 4s and 4p AOs of Cu, since the natural electron configuration of H and Cu in the $C_6H_5Cu\cdots(\eta^2\text{-}H_2)$ complex are $1s^{0.96}1p^{0.01}$ and $3d^{9.83}4s^{0.59}4p^{0.07}$, respectively.

Association of a second H_2 molecule with $C_6H_5Cu(\eta^2\text{-}H_2)$ leads to ten hyperconjugative interactions related to the $C_6H_5Cu\cdots(\eta^2\text{-}H_2)$ interaction (five for each H_2 molecule). These hyperconjugative interactions correspond to a total stabilization energy, $\Delta E(2)$, of more than 172 kcal mol^{-1}. Five hyperconjugative interactions between the C_6H_5Cu moiety and one out the two H_2 molecules of the $C_6H_5Cu(\eta^2\text{-}H_2)_2$ species along with the respective $\Delta E(2)$ values are shown in figure 4. The other five hyperconjugative interactions are exactly the same to those given in figure 4 for the $C_6H_5Cu(\eta^2\text{-}H_2)$ complex.

Let us now analyze the hyperconjugative interactions related to the $C_6H_5Cu\cdots(\eta^2\text{-}H_2)$ interaction in $C_6H_5Cu(\eta^2\text{-}H_2)_2$. The first hyperconjugative interaction arises from an electron density transfer from a LP NBO of d-type located on copper toward a BD* antibonding NBO of σ*-type on H_2 molecule stabilizing the system by almost 10 kcal mol^{-1}. The second hyperconjugative interaction is due to an electron density transfer from a partially occupied LP* of p-type AO on copper toward a BD* antibonding NBO of σ*-type on H_2 stabilizing the system by more than 20 kcal mol^{-1}. The fourth and fifth hyperconjugative interactions arise from electron density transfer from a bonding NBO of σ-type located on the H_2 molecule toward LP* NBOs located on copper. Finally, the fifth hyperconjugative interaction corresponds to a $\sigma(H\text{–}H) \rightarrow \sigma^*(C\text{–}Cu)$ electron transfer which probably accounts for the C–Cu bond elongation caused by H_2 coordination to Cu. As observed for $C_6H_5Cu(\eta^2\text{-}H_2)$, in $C_6H_5Cu(\eta^2\text{-}H_2)_2$, there is almost the same net electron density transfer of 0.066 | e| from each H_2 molecule (overall 0.132 |e|) toward the C_6H_5Cu moiety. The electron density is transferred from the 1σ MO of the H_2 molecules toward mainly the 4s and 4p AOs of copper.

For the $C_6H_5Cu(\eta^2\text{-}H_2)_3$ species, NBO analysis revealed a large number of hyperconjugative interactions taking place in the $C_6H_5Cu\cdots(\eta^2\text{-}H_2)$ interactions. The most significant among them shown in figure 4 could be classified into two groups: one group comprises hyperconjugative interactions relevant to the interactions involving the two structurally equivalent H_2 molecules, located below the carbocyclic ring plane, while the second group comprises hyperconjugative interactions relevant with the third H_2 molecule, located above the carbocyclic ring, exhibiting a slightly longer Cu–cd(H–H) distance compared to the other two H_2 ligands [figure 4(c)]. All these hyperconjugative interactions stabilize the system by about 247 kcal mol^{-1}. Inspection of figure 4 reveals that there are a number of hyperconjugative interactions with electron density transfer from $\sigma(H\text{–}H)$-type NBOs toward copper p-type NBOs as well as back-donation from copper d-type NBO toward antibonding $\sigma^*(H\text{–}H)$-type NBOs. In the $C_6H_5Cu(\eta^2\text{-}H_2)_3$ complex, there is an even higher electron density transfer from the 1σ MO of H_2 molecules toward the C_6H_5Cu moiety amounting to 0.29 |e| based on the natural charges upon comparing with the respective electron density transfer observed in $C_6H_5Cu(\eta^2\text{-}H_2)_2$ and $C_6H_5Cu(\eta^2\text{-}H_2)$.

To further delineate the nature of the $C_6H_5Cu\cdots(\eta^2\text{-}H_2)$ interactions, we employed AIM calculations for the representative $C_6H_5Cu(\eta^2\text{-}H_2)$, $C_6H_5Cu(\eta^2\text{-}H_2)_2$ and $C_6H_5Cu(\eta^2\text{-}H_2)_3$ species. The contour line maps of the Laplacian of the electron density, $\nabla^2 \rho_{BCP}$, for $C_6H_5Cu(\eta^2\text{-}H_2)$ is depicted in scheme 2, while similar diagrams are obtained for $C_6H_5Cu(\eta^2\text{-}H_2)_2$ and $C_6H_5Cu(\eta^2\text{-}H_2)_3$. In all cases, a BCP between the copper center and H_2 is observed, indicating that there is a bonding $C_6H_5Cu\cdots(\eta^2\text{-}H_2)$ interaction. To analyze this interaction, we calculated AIM parameters for three BCPs, the one found between C_6H_5Cu and the H_2 molecule, a second one found between the copper and the phenyl moiety, and a third found for the H–H bond in the H_2 molecule. These BCPs are denoted as $BCP_{(Cu\text{–}H2)}$, $BCP_{(C\text{–}Cu)}$, and $BCP_{(H\text{–}H)}$ (scheme 2).

According to Bader's [26] theory, the presence of a BCP between two atoms indicates bond formation. The values of certain parameters at BCPs are used in order to clarify the nature of the bond formed between two atoms. Thus, if the electron density at a BCP between two atoms, ρ_{BCP}, is large (>0.2 a.u.) and the value of its Laplacian, $\nabla^2 \rho_{BCP}$, is large and negative, then the bond formed is considered to be covalent. However, when TMs are present, the diffuse character of the electron distribution [32] leads to positive $\nabla^2 \rho_{BCP}$ values and small ρ_{BCP} values. Hence, Cortés-Guzmán and Bader suggested [12] that caution should be taken upon using the values of these two parameters to describe the delocalized

bonding encountered when TMs participate in the interaction. Consequently, a number of different parameters have been proposed to describe the bonding between two atoms within the framework of the AIM theory. Cremer and Kraka [33] proposed that a bond between two atoms could be considered as covalent if the value of the total energy density at the respective BCP, H_{BCP}, is negative. In addition, Espinosa *et al.* [34] based upon the value of the $|V_{BCP}|/G_{BCP}$ ratio, where V_{BCP} is the potential energy density at BCP and G_{BCP} is the kinetic energy density at BCP classified the bonding interactions into three categories as follows: (i) pure closed-shell interactions (e.g. ionic bonds, hydrogen bonds, and van der Waals interactions) characterized by $|V_{BCP}|/G_{BCP} < 1$ ($\nabla^2 \rho_{BCP} > 0$ and $H_{BCP} > 0$), (ii) pure open-shell (covalent) interactions characterized by $|V_{BCP}|/G_{BCP} > 2$ ($\nabla^2 \rho_{BCP} < 0$ and $H_{BCP} < 0$), and (iii) intermediate bonds with $1 < |V_{BCP}|/G_{BCP} < 2$ (i.e. $\nabla^2 \rho_{BCP} > 0$ and $H_{BCP} < 0$). Finally, Macchi and Sironi [32] outlined that a covalent bond involving TMs exhibits small $\nabla^2 \rho_{BCP}$ and ρ_{BCP} values, negative total energy density, $H_{BCP} < 0$ and G_{BCP}/ρ_{BCP} ratio lower than 1.

Let us examine first the values of the AIM parameters calculated for the $BCP_{(Cu–H2)}$. The values of the electron density, $\rho(\mathbf{r})$, and its Laplacian, $\nabla^2 \rho_{BCP}$, are 0.088 and 0.318. Accordingly, the $C_6H_5Cu\cdots(\eta^2\text{-}H_2)$ interaction could not be considered, as expected, as a purely covalent interaction. However, as mentioned above, when a TM is present in an interaction, then the values of both of these two parameters should be examined with caution [32] and a number of other parameters must be examined as well. Hence, the energy density H_{BCP} and the ratio H_{BCP}/ρ_{BCP} are −0.031 and −0.352, respectively, indicating a partially covalent
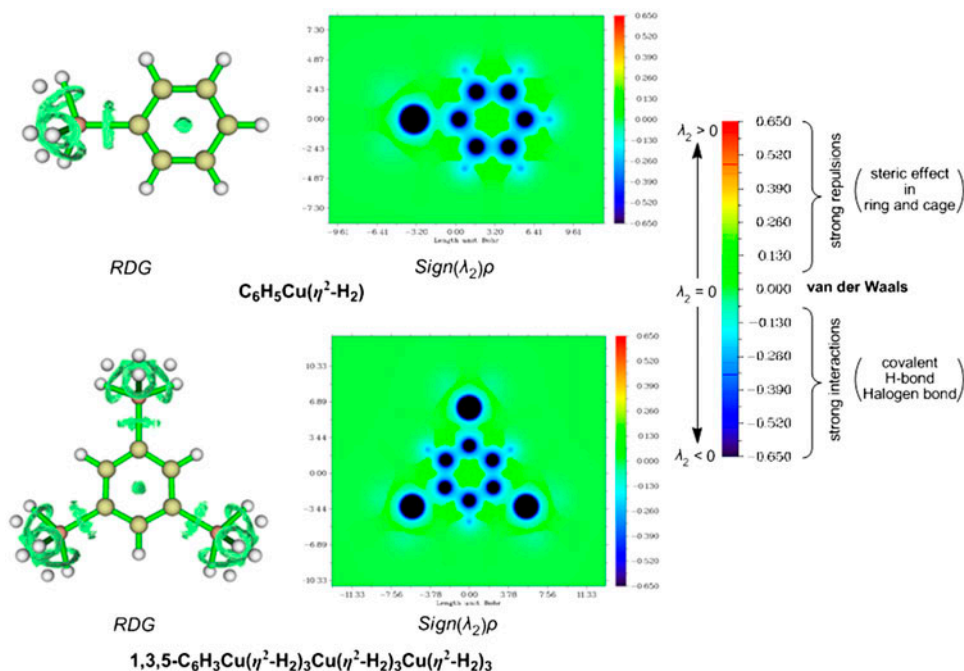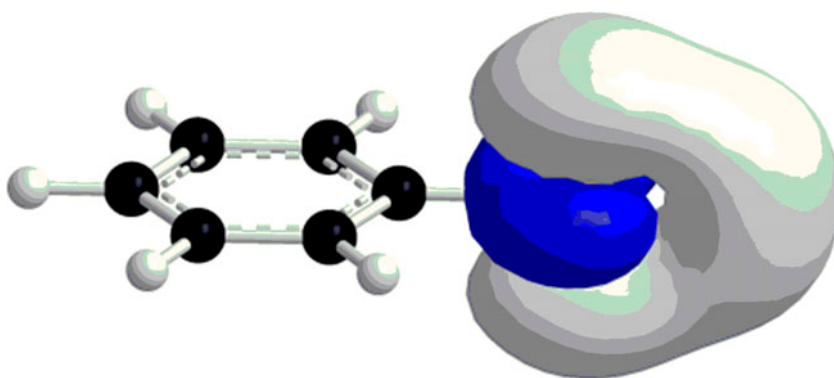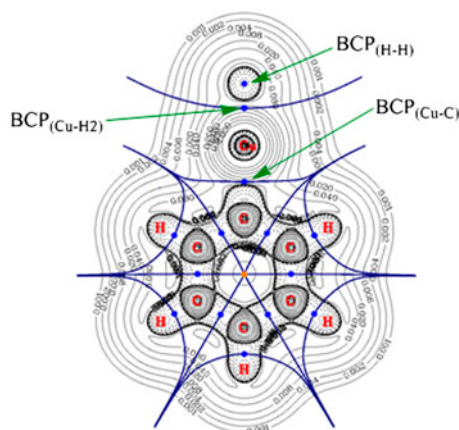

Figure 5.   Reduced density gradient 3-D plots (isosurface = 0.650) along with the 2-D plots of the Sign($\lambda_2(\mathbf{r})$)$\rho(\mathbf{r})$ function for $C_6H_5Cu(\eta^2\text{-}H_2)$ and $1,3,5\text{-}C_6H_3Cu(\eta^2\text{-}H_2)_3Cu(\eta^2\text{-}H_2)_3Cu(\eta^2\text{-}H_2)_3$ complexes calculated at the PBE0/Def2-QZVPP level.

Scheme 1.   3D plot of the 3c-2e bonding MO calculated by AdNDP method.

Scheme 2.   Contour line map of the Laplacian of the electron density, for the interaction of phenylcopper with a hydrogen molecule.

character for the $C_6H_5Cu\cdots(\eta^2$-$H_2)$ interaction. On the other hand, the $|V_{BCP}|/G_{BCP}$ ratio is 1.279 i.e., is between 1 and 2, and therefore, the $C_6H_5Cu\cdots(\eta^2$-$H_2)$ interaction is expected to exhibit character between covalent and ionic [34]. Finally, the G_{BCP}/ρ_{BCP} ratio of 1.247 is higher than 1, pointing to a closed-shell interaction (dispersion forces) between the copper and H_2. Overall, based upon the values of the AIM parameters on $BCP_{(Cu–H2)}$, we conclude that the respective $C_6H_5Cu\cdots(\eta^2$-$H_2)$ interaction exhibits a mixed covalent-ionic character involving also a component arising from intermolecular dispersion forces.

Attachment of a second H_2 molecule results in lowering of the $\rho(\mathbf{r})$ and it's Laplacian, $\nabla^2\rho_{BCP}$, which are 0.076 and 0.250, respectively. The same holds true for the H_{BCP} and the ratio H_{BCP}/ρ_{BCP} which are −0.024 and −0.316, respectively. The ratio $|V_{BCP}|/G_{BCP}$ is invariant at 1.279 while G_{BCP}/ρ_{BCP} ratio is 1.132, which is still higher than 1. Thus, the $C_6H_5Cu\cdots(\eta^2$-$H_2)$ interaction in $C_6H_5Cu(\eta^2$-$H_2)_2$ exhibits qualitatively the same character as in $C_6H_5Cu(\eta^2$-$H_2)$. Upon attaching a third H_2 molecule, we have further lowering of the AIM parameters on the $BCP_{(Cu–H2)}$, i.e., $\rho(\mathbf{r}) = 0.064$, $\nabla^2\rho_{BCP} = 0.209$, $H_{BCP} = -0.017$, H_{BCP}/ρ_{BCP} ratio is

-0.266, $|V_{BCP}|/G_{BCP}$ ratio is 1.243, and finally, the G_{BCP}/ρ_{BCP} ratio is 1.094. Therefore, once again attaching a H_2 molecule does not affect significantly the nature of the $C_6H_5Cu\cdots$ $(\eta^2\text{-}H_2)$ interaction. Taking into account that AIM parameters indicate the involvement of dispersion forces in the $C_6H_5Cu\cdots(\eta^2\text{-}H_2)$ interaction, we investigated further the RDG and the real space $Sign(\lambda_2(\mathbf{r}))\rho(\mathbf{r})$ function with promolecular approximation (figure 5).

The green disk-shaped RDGs around the $Cu\cdots(\eta^2\text{-}H_2)$ bond clearly demonstrate the weak van der Waals components of these interactions. This is further corroborated by the λ_2 term in the $Sign(\lambda_2(\mathbf{r}))\rho(\mathbf{r})$ function which is almost zero at the BCP of the $Cu\cdots(\eta^2\text{-}H_2)$ bond. Furthermore, both the RDGs and λ_2 terms illustrate the metallophilic interactions whenever possible.

4. Concluding remarks

In this work, we have investigated by means of DFT calculations the hydrogen storage capacity of C_6H_5Cu and $1,3,5\text{-}Cu_3C_6H_3$ and found that these molecules fulfill the US DOE target requirements for low-cost hydrogen storage materials. A thorough analysis of the $Cu\cdots(\eta^2\text{-}H_2)$ interactions by a multitude of electronic structure calculation methods (NBO, AIM, ELF, RDG, and $Sign(\lambda_2(\mathbf{r}))\rho(\mathbf{r})$ functions) showed that the $Cu\cdots(\eta^2\text{-}H_2)$ interactions exhibit a mixed covalent-ionic character accompanied by weak intermolecular dispersion interactions as well.

Supplementary material

Cartesian Coordinates and energies (in Hartrees) of the $C_6H_5Cu(\eta^2\text{-}H_2)_n$ and $C_6H_3Cu(\eta^2\text{-}H_2)_nCu(\eta^2\text{-}H_2)_nCu(\eta^2\text{-}H_2)_n$ ($n = 1$–3) (table S1). These data can be obtained free of charge via http://www.ccdc.cam.ac.uk/conts/retrieving.html.

Disclosure statement

No potential conflict of interest was reported by the authors.

Supplemental data

The supplementary material for this paper is available online at http://dx.doi.org/10.1080/00958972.2015.1064906.

References

[1] (a) A. Züttel. *Mater. Today*, **6**, 24 (2003); (b) G.W. Crabtree, M.S. Dresselhaus, M.V. Buchanan. *Phys. Today*, **57**, 39 (2004); (c) R. Coontz, B. Hanson. *Science*, **305**, 957 (2004); (d) W. Lubitz, W. Tumas. *Chem. Rev.*, **107**, 3900 (2007); (e) L.G. Hector Jr., J.F. Herbst. *J. Phys.: Condens. Matter*, **20**, 064229 (2008); (f) S. Giri, S. Bandaru, A. Chakraborty, P.K. Chattaraj. *Phys. Chem. Chem. Phys.*, **13**, 20602 (2011); (g) U.B. Demirci, P. Miele. *Energy Environ. Sci.*, **4**, 3334 (2011); (h) S. Pan, S. Banerjee, P.K. Chattaraj. *J. Mex. Chem. Soc.*, **56**, 229 (2012); (i) S. Giri, F. Lund, A.S. Núñez, A. ChaToro-Labbé. *J. Phys. Chem. A*, **117**, 5544 (2013).
[2] (a) M. Hirscher. *Handbook of Hydrogen Storage: New Materials for Future Energy Storage*, Wiley-VCH Verlag GmbH & Co. KGaA, Winheim (2010); (b) L. Schlapbach, A. Züttel. *Nature*, **414**, 353 (2001); (c) L. Schlapbach. *MRS Bull.*, **27**, 675 (2002) and other articles in this special issue; (d) R.H. Jones, G.J. Thomas. *Materials for the Hydrogen Economy*, CRC Press, Boca Raton (2008); (e) A. Züttel, A. Borgschulte, L.

Schlapbach. *Hydrogen as a Future Energy Carrier*, Wiley-VCH Verlag GmbH & Co. KGaA, Weinheim (2008); (f) R.B. Gupta. *Hydrogen Fuel: Production, Transport, and Storage*, CRC Press, Boca Raton (2009).

[3] US DOE EERE Fuel cell technologies program. Available online at: http://www1.eere.energy.gov/hydrogenandfuelcells/

[4] (a) G.J. Kubas. *Science*, **314**, 1096 (2006); (b) G.J. Kubas. *J. Organomet. Chem.*, **635**, 37 (2001).

[5] H. Lee, B. Huang, W. Duan. *J. Ihm. Phys. Rev. B*, **82**, 085439 (2010) and references therein.

[6] Y.-H. Kim, Y. Zhao, A. Williamson, M.J. Heben, S.B. Zhang. *Phys. Rev. Lett.*, **96**, 016102 (2006).

[7] (a) H. Imamura, K. Masanari, M. Kusuhara, H. Katsumoto, T. Sumi, Y. Sakata. *J. Alloys Compd.*, **386**, 211 (2005); (b) L. Zaluski, A. Zaluska, J.O. Strom-Olsen. *J. Alloys Compd.*, **253**, 70 (1997); (c) G. Liang, J. Huot, S. Boily, A. Van Neste, R. Schulz. *J. Alloys Compd.*, **291**, 295 (1999).

[8] I. Infante, L. Gagliardi, X. Wang, L. Andrews. *J. Phys. Chem. A*, **113**, 2446 (2009).

[9] S. Giri, F. Lund, A.S. Núñez, A. Toro-Labbé. *J. Phys. Chem. C*, **117**, 5544 (2013).

[10] K. Reich. *Compt. Rend.*, **177**, 322 (1923).

[11] (a) H. Gilman, J.M. Straley. *Recl. Trav. Chim. Pays-Bas*, **55**, 821 (1936); (b) H. Gilman, R.G. Jones, L.A. Woods. *J. Org. Chem.*, **17**, 1630 (1952); (c) H. Gilman, L.A. Woods. *J. Am. Chem. Soc.*, **65**, 435 (1943); (d) F.A. Bolth, W.M. Whaley, E.B. Starkey. *J. Am. Chem. Soc.*, **65**, 1456 (1943); (e) F.A. Bolth, W.M. Whaley, E.B. Starkey. *J. Am. Chem. Soc.*, **68**, 793 (1946); (f) J.C. Warf. *J. Am. Chem. Soc.*, **74**, 3702 (1952).

[12] F. Cortés-Guzmán, R.F.W. Bader. *Coord. Chem. Rev.*, **249**, 633 (2005).

[13] (a) E. Krause, B. Wendt. *Chem. Ber.*, **56**, 2064 (1923); (b) R. Reich. *C. R. Acad. Sci. Paris*, **177**, 322 (1923); (c) H. Hasizimoto, T. Nakano. *J. Org. Chem.*, **31**, 891 (1966).

[14] C.D.M. Beverwijk, G.J.M. van der Kerk, A.J. Leusink, J.G. Noltes. *Organomet. Chem. Rev. A*, **5**, 215 (1970).

[15] S. Sun, X. Xing, H. Liu, Z. Tang. *J. Phys. Chem. A*, **109**, 11742 (2005).

[16] X.-J. Liu, X. Zhang, K.-L. Han, X.-P. Xing, S.-T. Sun, Z. Tang. *J. Phys. Chem. A*, **111**, 3248 (2007).

[17] X.-J. Liu, C.-L. Yang, X. Zhang, K.-L. Han, Z.-C. Tang. *J. Comput. Chem.*, **29**, 1667 (2008).

[18] (a) A.C. Tsipis. *Organometallics*, **31**, 7206 (2012); (b) A.C. Tsipis, D.N. Gkarmpounis. *J. Mol. Model.*, **21**, 153 (2015).

[19] M.J. Frisch, G.W. Trucks, H.B. Schlegel, G.E. Scuseria, M.A. Robb, J.R. Cheeseman, J.A. Montgomery Jr., T. Vreven, K.N. Kudin, J.C. Burant, J.M. Millam, S.S. Iyengar, J. Tomasi, V. Barone, B. Mennucci, M. Cossi, G. Scalmani, N. Rega, G.A. Petersson, H. Nakatsuji, M. Hada, M. Ehara, K. Toyota, R. Fukuda, J. Hasegawa, M. Ishida, T. Nakajima, Y. Honda, O. Kitao, H. Nakai, M. Klene, X. Li, J.E. Knox, H.P. Hratchian, J.B. Cross, V. Bakken, C. Adamo, J. Jaramillo, R. Gomperts, R.E. Stratmann, O. Yazyev, A.J. Austin, R. Cammi, C. Pomelli, J.W. Ochterski, P.Y. Ayala, K. Morokuma, G.A. Voth, P. Salvador, J.J. Dannenberg, V.G. Zakrzewski, S. Dapprich, A.D. Daniels, M.C. Strain, O. Farkas, D.K. Malick, A.D. Rabuck, K. Raghavachari, J.B. Foresman, J.V. Ortiz, Q. Cui, A.G. Baboul, S. Clifford, J. Cioslowski, B.B. Stefanov, G. Liu, A. Liashenko, P. Piskorz, I. Komaromi, R.L. Martin, D.J. Fox, T. Keith, M.A. Al-Laham, C.Y. Peng, A. Nanayakkara, M. Challacombe, P.M.W. Gill, B. Johnson, W. Chen, M.W. Wong, C. Gonzalez, J.A. Pople, *Gaussian 09, Revision B.01*, Gaussian, Inc., Wallingford, CT (2010).

[20] (a) J.P. Perdew, K. Burke, M. Ernzerhof. *Phys. Rev. Lett.*, **77**, 3865 (1996); (b) M. Ernzerhof, G.E. Scuseria. *J. Chem. Phys.*, **110**, 5029 (1999); (c) C. Adamo, V. Barone. *Chem. Phys. Lett.*, **274**, 242 (1997); (d) C. Adamo, V. Barone. *J. Chem. Phys.*, **110**, 6160 (1999); (e) C. Adamo, G.E. Scuseria, V. Barone. *J. Chem. Phys.*, **111**, 2889 (1999); (f) C. Adamo, V. Barone. *Theor. Chem. Acc.*, **105**, 169 (2000); (g) V. Vetere, C. Adamo, P. Maldivi. *Chem. Phys. Lett.*, **325**, 99 (2000).

[21] (a) P. Hirva, M. Haukka. *J. Mol. Model.*, **14**, 171 (2008); (b) J. Graciani, A.M. Márquez, J.J. Plata, Y. Ortega, N.C. Hernández, A. Meyer, C.M. Zicovich-Wilson, J.F. Sanz. *J. Chem. Theory Comput.*, **7**, 56 (2011); (c) L.F. Pašteka, T. Rajsky, M. Urbana. *J. Phys. Chem.*, **117**, 4472 (2013); (d) M. Steinmetz, S. Grimme. *Chem. Open*, **2**, 115 (2013).

[22] F. Weigend, R. Ahlrichs. *Phys. Chem. Chem. Phys.*, **7**, 3297 (2005).

[23] (a) A.E. Reed, L.A. Curtiss, F. Weinhold. *Chem. Rev.*, **88**, 899 (1988); (b) F. Weinhold. In *The Encyclopedia of Computational Chemistry*, P.R. Schleyer (Ed.), p. 1792, Wiley, Chichester (1998); (c) NBO 6.0.. E.D. Glendening, J.K. Badenhoop, A.E. Reed, J.E. Carpenter, J.A. Bohmann, C.M. Morales, C.R. Landis, F. Weinhold, *Theoretical Chemistry Institute*, University of Wisconsin, Madison (2013).

[24] R. Ditchfield. *Mol. Phys.*, **27**, 789 (1974).

[25] J. Gauss. *J. Chem. Phys.*, **99**, 3629 (1993).

[26] (a) R.F.W. Bader. *Atoms in Molecules – A Quantum Theory*, Oxford University Press, Oxford (1990); (b) R.F.W. Bader. *J. Phys. Chem. A*, **102**, 7314 (1998).

[27] (a) T. Lu, F. Chen. *J. Comput. Chem.*, **33**, 580 (2012); (b) T. Lu, F. Chen. *J. Mol. Graph. Model.*, **38**, 314 (2012).

[28] D.Y. Zubarev, A.I. Boldyrev. *Phys. Chem. Chem. Phys.*, **10**, 5207 (2008).

[29] S.A. Shevlin, Z.X. Guo. *Chem. Soc. Rev.*, **38**, 211 (2009).

[30] J. Yang, A. Sudik, C. Wolverton, D.J. Siegel. *Chem. Soc. Rev.*, **39**, 656 (2010).

[31] G.J. Kubas. *Chem. Rev.*, **107**, 4152 (2007).

[32] P. Macchi, A. Sironi. *Coord. Chem. Rev.*, **238–239**, 383 (2003).

[33] D. Cremer, E. Kraka. *Angew. Chem. Int. Ed. Engl.*, **23**, 627 (1984).

[34] E. Espinosa, I. Alkorta, J. Elguero, E. Molins. *J. Chem. Phys.*, **117**, 5529 (2002).